Applied Catalysis B: Environmental 204 (2017) 430–439

Contents lists available at ScienceDirect

Applied Catalysis B: Environmental

journal homepage: www.elsevier.com/locate/apcatb

Selective photocatalytic oxidation of 5-hydroxymethyl-2-furfural to 2,5-furandicarboxyaldehyde in aqueous suspension of g-C_3N_4

Igor Krivtsov[a,b], Elisa I. García-López[c,*], Giuseppe Marcì[c], Leonardo Palmisano[c], Zakariae Amghouz[d], José R. García[a], Salvador Ordóñez[e], Eva Díaz[e]

[a] Department of Organic and Inorganic Chemistry, University of Oviedo-CINN, 33006 Oviedo, Spain
[b] Nanotechnology Education and Research Center, South Ural State University, 454080, Chelyabinsk, Russia
[c] "Schiavello-Grillone" Photocatalysis Group. Dipartimento di Energia, Ingegneria dell'informazione e modelli Matematici (DEIM), Università di Palermo, Viale delle Scienze, 90128 Palermo, Italy
[d] Servicios Científico Técnicos, Universidad de Oviedo, 33006 Oviedo, Spain
[e] Department of Chemical and Environmental Engineering, University of Oviedo, 33006 Oviedo, Spain

ARTICLE INFO

Article history:
Received 14 October 2016
Received in revised form
21 November 2016
Accepted 22 November 2016
Available online 23 November 2016

Keywords:
Carbon nitride
Exfoliation
Partial photocatalytic oxidation
5-Hydroxymethyl-2-furfural
2,5-Furandicarboxaldehyde

ABSTRACT

Graphitic carbon nitride assisted partial photocatalytic oxidation of 5-hydroxymethyl-2-furfural (HMF) in aqueous medium was investigated. Different carbon nitride precursors were considered, being melamine the one yielding the most efficient photocatalyst. The obtained 30% selectivity of HMF oxidation to 2,5-furandicarboxaldehyde (FDC) is higher than those reported up to now. A further thermal exfoliation of the g-C_3N_4 samples showed under artificial light irradiation both an enhanced photocatalytic activity in conversion of HMF, and selectivity (ca. 42–45%) to FDC. The performance of the catalysts increased when the experiments were carried out under real outdoor illumination, reaching 50% of selectivity versus FDC formation at 40% of HMF conversion. The utilization of radical scavengers revealed that $O_2^{\bullet -}$ was the main reactive species responsible for HMF oxidation to FDC. The photocatalytic test carried out under natural solar irradiation resulted in higher yields of FDC compared to that observed in the laboratory UV irradiated set-up, thus demonstrating the applicability of the exfoliated carbon nitride material in real-life conditions.

1. Introduction

The use of renewable feedstock for producing valuable chemicals and materials is a key point of the modern sustainable industry. Saccharides deriving from lignocellulose hydrolysis are one of the most abundant biomass-derived platform molecules [1]. The oxidation of six-carbons sugars yields 5-hydroxymethyl-2-furfural (HMF), which can be furtherly converted to 2,5-furandicarboxaldehyde (FDC) and 2,5-furandicarboxylic acid (FDCA), the precursors for biopolymers fabrication [2–4]. Several approaches for HMF oxidation, utilizing noble metals [5–7] or transition metal phosphates [8,9] as catalysts, have been explored. However, the application of high temperatures, as well as expensive noble metals [5] makes this process energy-consuming and environmentally unfriendly. Heterogeneous photocatalysis provides a greener alternative to many widely applied catalytic oxidation reactions because toxic by-products are not formed and in principle solar radiation could be used. Highly selective oxidation of aromatic alcohols to aldehydes over TiO_2-based photocatalysts has been extensively explored [10–12], although in most cases the reactions have been carried out in organic media [13–15]. Titanium dioxide under UV irradiation readily forms hydroxyl radicals, which can unselectively attack organic species until their mineralization to CO_2 and H_2O occurs. The oxidant properties of TiO_2 are exalted by the relatively lower stability of the pentatomic furanic ring compared to the hexatomic aromatic structures, and consequently it is not surprising that the highest selectivity of HMF photooxidation to FDC achieved so far is only 22% [16]. A photocatalytic material with appropriate thermodynamic requirements, which has recently attracted attention to perform selective oxidations, is graphitic carbon nitride (g-C_3N_4). It is normally prepared by thermal condensation of dicyandiamide, melamine, urea or thiourea [17]. Relatively low specific surface areas (SSA), in the range 4–7 $m^2\,g^{-1}$, are obtained if thiourea or melamine are used as the precursors, although values close to 70 $m^2\,g^{-1}$ (but with very low yields) have been reported for samples prepared at high condensa-

* Corresponding author.
E-mail address: elisaisabel.garcialopez@unipa.it (E.I. García-López).

http://dx.doi.org/10.1016/j.apcatb.2016.11.049
0926-3373/

tion temperatures [18–20]. There are two general ways to increase the SSA of g-C_3N_4: hard or soft templating during the synthesis [21] and post-synthetic exfoliation [22]. Hard templating demands the elimination of the structure-directing material, usually a mesoporous silica, by its dissolution in hazardous hydrofluoric acid, while the presence of soft templates during the preparation might result in the formation of undesired carbonaceous residue [21]. Liquid exfoliation successfully enhances the specific surface area of carbon nitride; however, it usually implies the application of toxic oxidative agents or aggressive media [23]. Recently, Niu et al. [24] have reported an easy thermal exfoliation method allowing to reach values of specific surface area up to ca. 300 $m^2\,g^{-1}$.

The unique electronic structure of carbon nitride semiconductor triggered its application in the field of organic compounds conversion by selective photocatalytic oxidation [25] such as partial photooxidation of amines [26], aromatic hydrocarbons [27–29], cyclohexane [30] and aromatic alcohols with molecular oxygen [31–35]. To the best of our knowledge, despite the favourable position of its energy levels and the absence of hydroxyl groups on the surface, which would favour the direct formation of the unselective OH• radicals, carbon nitride has not been utilized before for selective oxidation of non-aromatic alcohols in aqueous medium. In the present work it is reported the partial photo-oxidation of HMF in aqueous medium aimed to obtain FDC by using both as-prepared and thermally exfoliated g-C_3N_4 samples. The overall partial oxidation of HMF to FDC by using carbon nitride is also shown in Scheme 1.

2. Experimental

2.1. Photocatalyst preparation

Bulk carbon nitride (g-C_3N_4) samples were prepared *via* the thermal condensation method from different precursors as before reported [18,19]. 10 g of melamine, 20 g of urea or 10 g of thiourea were placed in a ceramic crucible covered with a lid and heated in a muffle furnace at 2 °C min^{-1} up to 520 °C, then left for 2 h at the reached temperature and slowly cooled down. The g-C_3N_4 samples derived from the different sources, melamine, urea and thiourea, were labelled as MCN, UCN and TuCN, respectively. The bulk carbon nitride prepared from melamine (MCN) was used as the precursor for the thermally exfoliated g-C_3N_4 nanosheets [24,36]. To this purpose, 6 g of bulk carbon nitride were powdered in a mortar, evenly spread on the bottom of a ceramic bowl with a diameter of 14 cm, calcined in a static air atmosphere at 450, 500, 520 and 540 °C by using a temperature ramp of 2 °C min^{-1} and maintained for 4 h at each of the final temperatures. The thermally exfoliated carbon nitride samples were coded as MCN_450, MCN_500, MCN_520, MCN_540.

2.2. Photocatalysts characterization

The crystalline structure of the samples was determined at room temperature by powder X-ray diffraction analysis (PXRD) carried out by using a Panalytical Empyrean apparatus, equipped with CuKα radiation source and PixCel1D (tm) detector. Specific surface areas (SSA) were calculated in accordance with the standard Brunauer-Emmet-Teller (BET) method from the nitrogen adsorption data using a Micromeritics ASAP 2020. Infrared spectra of the samples in KBr (Aldrich) pellets were recorded with 4 cm^{-1} resolution and 256 scans using a FTIR-8400 Shimadzu spectrometer. Diffuse reflectance spectra (DRS) were obtained in air at room temperature in the 250–800 nm wavelengths range by means of a Shimadzu UV-2401 PC spectrophotometer, with $BaSO_4$ as the reference material. Mettler Toledo TGA/SDTA851 was used to investigate the thermal decomposition of g-C_3N_4 under an O_2 flow of 50 mL min^{-1} in the temperature range 25–1000 °C. The binding energies of C, N and O in the pristine and exfoliated MCN samples were measured by X-ray Photoelectron Spectroscopy (XPS) by using a SPECS system equipped with a Hemispherical Phoibos detector operating in a constant pass energy, using MgKα radiation ($h{\cdot}\nu$ = 1253.6 eV). TEM studies were performed on a JEOL JEM-2100F transmission electron microscope operated at an accelerating voltage of 200 kV, equipped with a field emission gun (FEG) and an ultra-high resolution pole-piece that provided a point-resolution better than 0.19 nm. The samples for TEM were dispersed in ethanol, sonicated and sprayed on a holey carbon film coated copper grid and then allowed to air-dry; finally, Gatan SOLARUS 950 was used before carrying out observations with the microscope.

2.3. Photocatalytic set-up and procedure

The irradiation experiments were carried out in a Pyrex cylindrical photoreactor (internal diameter: 32 mm, height: 188 mm) containing 150 mL of aqueous suspension, irradiated by six external Actinic BL TL MINI 15 W/10 Philips fluorescent lamps emitting in the 340–420 wavelength range with the main emission peak at 365 nm. The reaction was carried out at about 25 °C as the reactor open to the atmosphere was provided by a thimble where water was allowed to circulate. Selected experiments were carried out in anaerobic condition by continuously bubbling N_2 throughout the runs to estimate the influence of O_2 on the reaction. The initial HMF concentration was 0.5 mM at the natural pH. The amount of solid photocatalyst used for the experiments was 50 mg, except for the pristine carbon nitrides MCN, UCN, TuCN and MCN_450, for which 100 mg were used, due to their poorer light absorbance compared to the other samples. In this way, all the entering photons were virtually absorbed by the suspension. The impinging radiation energy in the range 315–400 nm was measured by a radiometer Delta Ohm DO9721 with an UVA probe and its average value was 3.4 W m^{-2}. Some experiments were performed by reusing one of the best materials (MCN_520) in order to verify its performance in a series of four consecutive runs. Details on the procedure for the experiments of re-utilization are reported in the Supporting information. Selected scavengers were used in order to establish the reactive species responsible for HMF conversion and the selectivity to FDC. Sodium formate (HCOONa) was used as a hole scavenger, *tert*-butyl alcohol (*t*-BuOH) as an OH• radical scavenger, copper (II) chloride dihydrate to trap electrons, and *p*-benzoquinone to scavenge $O_2^{\bullet-}$ radicals. The concentration of sodium formate and *tert*-butyl alcohol scavengers was 5 mM, whereas for $CuCl_2$ and *p*-benzoquinone the concentration was reduced to 1 mM, which enabled to avoid the precipitation of copper hydroxide during the photocatalytic run and to decrease the effect of the formed *p*-hydroxiquinone on the light absorbance by the suspension.

Samples of the irradiated solution were withdrawn at fixed time intervals and immediately filtered through 0.25 μm membranes (HA, Millipore) to separate the photocatalyst particles. Liquid aliquots were analysed by a Thermo Scientific Dionex UltiMate 3000 HPLC equipped with a Diode Array detector to identify and to determine the concentration of HMF, FDC and 5-formyl-2-furoic acid (FFA). A REZEK ROA Organic acid H^+ column was used with a mobile phase of aqueous 2.5 mM H_2SO_4 solution at a flow rate of 0.6 mL min^{-1}. Standards purchased from Sigma-Aldrich with a purity >99% were used to identify the products formed during the reaction and to obtain the calibration curves. Additionally, the reaction products were identified and selectivity values were confirmed by a GC–MS technique, using a Shimadzu 2100 Ultra GC–MS equipped with a Teknokroma TRB-5MS (95%) dimethyl (5%) diphenylpolysiloxane copolymer column.

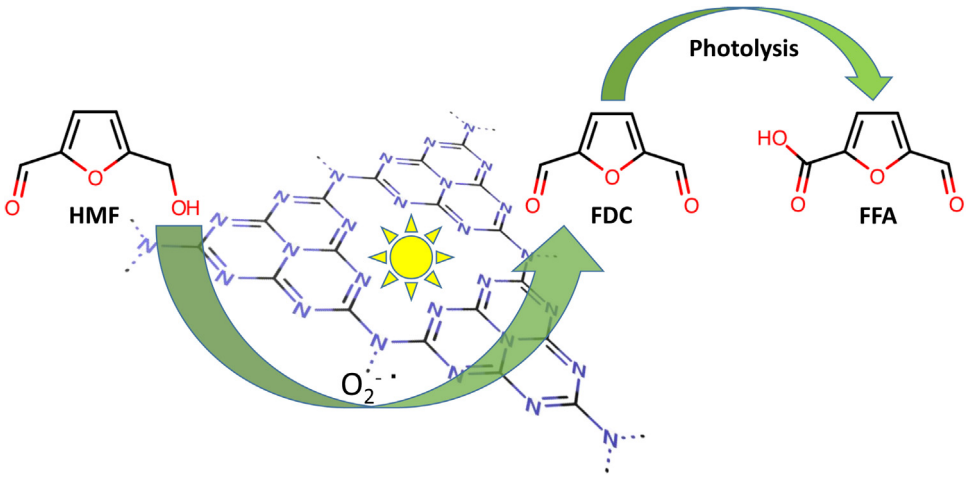

Scheme 1. Photocatalytic oxidation of HMF to FDC by using carbon nitride as photocatalyst along with the photolysis reaction of FDC producing FFA.

The photocatalytic reactions under a natural solar irradiation were carried out on clear sunny days of 6th, 9th and 18th May, 2016 in Palermo (Italy) from 9:30 to 13:30. Typically, 75 mL of 0.5 mM HMF solution and 25 mg of MCN_520 and MCN_540 samples were introduced inside a round-shaped Pyrex batch reactor having a total volume of 125 mL and a diameter of 10 cm. The reactor was closed and no gases were fed during the tests as preliminary experiments indicated that O_2 deriving from air and present in the system was sufficient to induce the oxidation. The suspensions of the carbon nitride samples in HMF solution were continuously magnetically stirred and approximately 2.5 mL were withdrawn every 30 min and analysed by using the previously described analytical procedure. The photon flux was measured every 10 min throughout the photocatalytic tests. Moreover, selected additional experiments were carried out by using MCN_520 and MCN_540 photocatalysts under solar light filtered by means of 1 M $NaNO_2$ solution ($\lambda > 400$ nm).

3. Results and discussion

3.1. Bulk g-C_3N_4 derived from the different precursors

3.1.1. Properties of bulk g-C_3N_4

It is known that the thermal condensation of the different carbon nitride precursors can significantly influence the structure and properties of g-C_3N_4. In the present case the yields of g-C_3N_4 obtained from melamine, urea and thiourea were approximately 60, 5, and 10 wt%, respectively. The two main diffraction maxima for g-C_3N_4 at 13° and 27°, reported in Fig. 1(A) can be attributed to (100) and (002) crystallographic planes of g-C_3N_4. These results are consistent with the studies reported before [18,19]. The variation of the intensity of the mentioned diffraction peaks, along with the slightly more pronounced reflections at 46.2 and 56.4 angles, assigned to (300) and (004) crystallographic planes, corresponding to the tri-s-triazine network [37], could be an indication of the degree of polymerization of g-C_3N_4, which decreases in the order MCN > TuCN > UCN.

FTIR spectroscopy of these solids confirmed the carbon nitride structure of the materials, showing no significant differences among the samples synthesized using different precursors (Supporting information, Fig. S1). UV–vis spectroscopy indicated significant discrepancies in their light absorption properties. The typical band-gap value of carbon nitride (2.73 eV) was found for the MCN sample, whilst a significant blue-shift occurred for the UCN one (2.86 eV band-gap) (Supporting information, Fig. S2), which can be attributed to its lower polymerization degree, hypothesized on the basis of PXRD results. The incorporation of S-heteroatom into the TuCN carbon nitride sample, extended the light absorption to the visible region resulting in a slight decrease of its band-gap value to 2.71 eV and the appearance of the sub-band-gap was estimated to be 2.17 eV. The low specific surface area generally observed for g-C_3N_4 materials is a drawback which could prevent their utilization as (photo)catalysts. This property depends on the precursor selected for their preparation, as shown in Table 1 and in the N_2 adsorption-desorption isotherms reported in Fig. S3. The higher SSA of UCN sample could be a consequence of a polymerization mechanism different from that of the other samples, resulting in the formation of a less condensed network, as suggested by the PXRD study.

3.1.2. Photocatalytic oxidation of HMF by using bulk g-C_3N_4

The extent of adsorption and photolysis of the substrate was determined before discussing the photoreactivity results. The adsorption of 0.5 mM HMF or FDC on the surface of the solid did not exceed 1% of the initial concentration and it can be considered negligible. On the contrary, the photolytic decomposition of HMF under UV illumination for 4 h was about 6%, but no formation of FDC was observed (Fig. S4). The photolytic stability of FDC under irradiation was lower than that of HMF, in fact, almost 20% was degraded after 4 h, and unlike the substrate, its photolysis produced FFA in large quantities (Fig. S4). Preliminary photocatalytic tests carried out in the presence of increasing amounts of MCN, from 25 to 200 mg, indicated that the optimum amount of photocatalyst was 100 mg (Fig. S5). By considering that all of the prepared materials possess similar light absorption, this amount was chosen also for the other two samples. The conversion of HMF versus irradiation time and the formation of FDC are reported in Fig. 2(A) and (B), respectively. The highest activity was observed for UCN sample, while the lowest one for TuCN, which could be related to the SSA values of the solids. The amount of FDC formed during the reaction was very similar for MCN and UCN, which implies that the selectivity to FDC formation was higher for MCN, as shown in Fig. 2(C). In addition to the influence of SSA, the bulk properties of the photocatalyst can also play some role on the reaction performance. The similar dependence of selectivity to FDC versus the HMF conversion observed for MCN and TuCN, as shown in Fig. 2(D), suggests that the bulk structure (determining the band positions) of these two materials which appeared to be similar according to the PXRD and spectroscopic data, was also responsible for the high selectivity to FDC formation. Thermal condensation of urea *via* a different pathway due to the presence of oxygen in the starting molecule, led to the formation of less polymerized carbon nitride network, resulting in poorer efficiency of

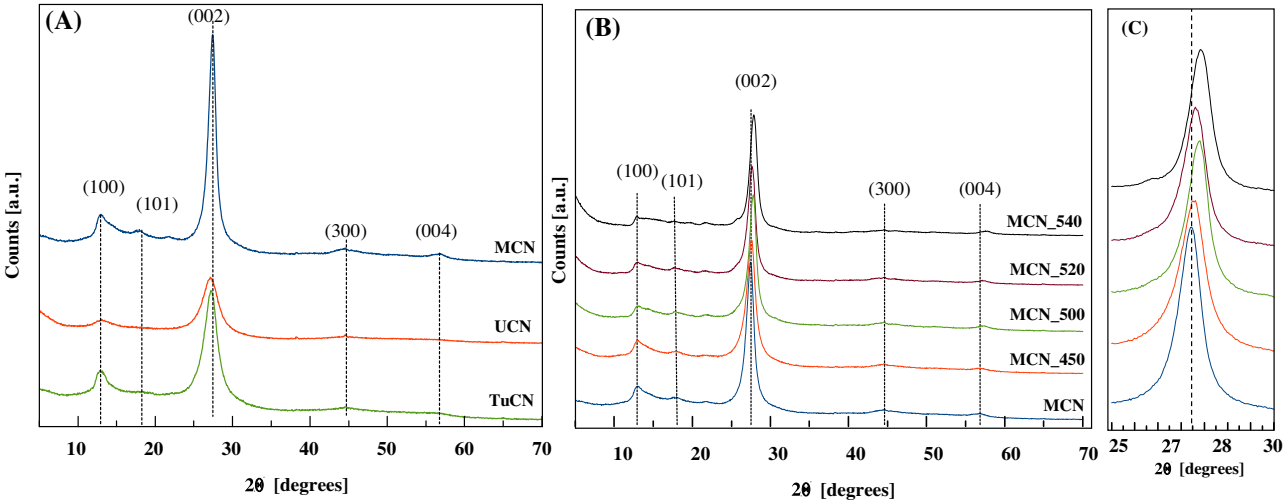

Fig. 1. PXRD patterns of (A): (—) MCN, (—) UCN, (—) TuCN samples and (B): thermo-exfoliated carbon nitride samples, i.e. Pristine MCN (—) and thermally exfoliated MCN_450 (—), MCN_500 (—), MCN_520 (—) and MCN_540 (—) samples. (C) Enlargement of the (002) in Fig. 1 (B).

Table 1
Specific surface area (SSA), band gap, HMF initial conversion rate (r), HMF conversion after 4 h of irradiation and selectivity to FDC formation at 30% of HMF conversion.

Sample	SSA [$m^2 g^{-1}$]	Band gap [eV]	HMF initial conversion rate, r [mM min^{-1}]	HMF Conversion (%)	FDC Selectivity (%)
UCN	28	2.86	0.0012	44	22
TuCN	4.0	2.71	0.0007	26	27[c]
MCN	7.0	2.73	0.0009	39	28
MCN_450	14	2.75	0.0010	38	37
MCN_500	154	2.78	0.0015	52	42
MCN_520	161	2.79	0.0018/0.0033[a]/0.0009[b]	58/81[a]/31[b]	44/47[a]/47[b]
MCN_540	169	2.90	0.0025/0.0091[a]/0.0012[b]	69/>99[a]/42[b]	43/49[a]/53[b]

[a] The value for the HMF photooxidation test under solar light.
[b] The value for the HMF photooxidation test under solar light in the presence of a 1 M $NaNO_2$ filter.
[c] The value is shown for 25% of HMF conversion.

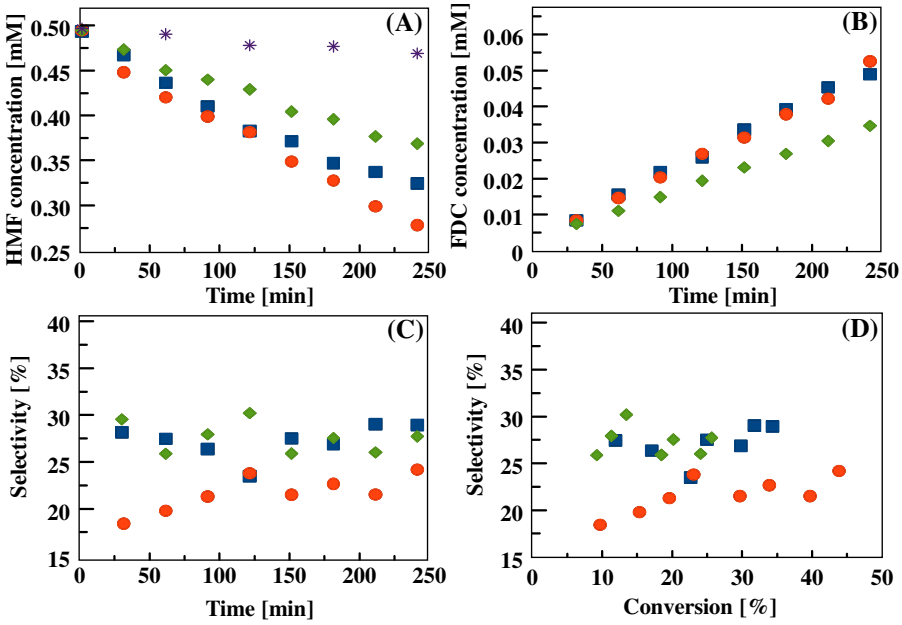

Fig. 2. HMF degradation (A); formation of FDC (B); selectivity to FDC versus irradiation time (C) and selectivity of the reaction to FDC versus HMF conversion (D) in the presence of MCN (■), UCN (●), and TuCN (◆) samples. (*) HMF photolysis in the homogeneous system.

the UCN sample in the partial photooxidation, as shown on Fig. 2(C) and (D).

A run carried out for the sake of comparison in the presence of TiO_2 Evonik P25, not reported in Fig. 2, indicated that this catalyst was able to degrade HMF almost completely in 4 h but the selectivity to FDC was virtually zero at any time of the runs.

As above mentioned, the formation of FFA was found during the photolysis of FDC. The same compound in small amounts was also

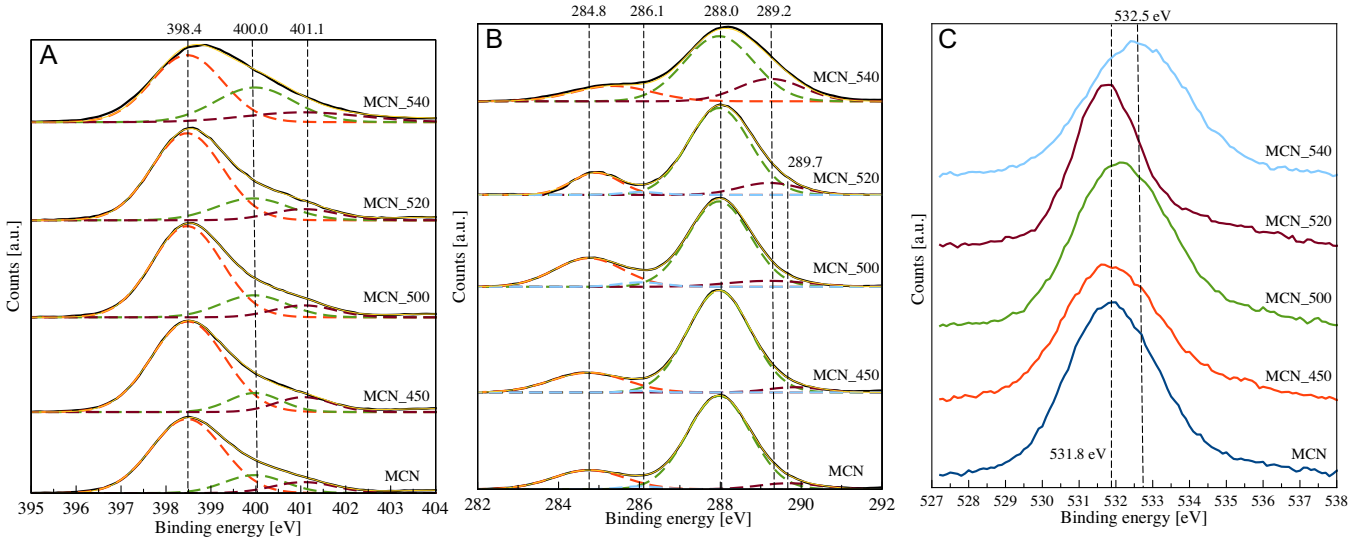

Fig. 3. XPS spectra of N 1s (A), C 1s (B) and O 1s (C) regions of the MCN and thermally exfoliated samples.

observed during the photocatalytic reactions of HMF conversion. Notably, its content did not depend on the type of the photocatalyst used for the reaction, but it was related to the FDC concentration. Therefore, the formation of FFA can be attributed to the photolysis of FDC deriving from the photooxidation of HMF (Fig. S6).

3.2. Photocatalytic conversion of HMF by using thermally exfoliated carbon nitride samples

3.2.1. Properties of the exfoliated g-C_3N_4

The preparation of carbon nitride using melamine as the precursor is preferable because it can be obtained in high yields and the selectivity for the partial photooxidation of HMF to FDC by using this photocatalyst was also high. In general, the changes caused by the thermal exfoliation follow the trends described in Refs. [23], and [34]. The diffraction patterns of the thermo-exfoliated samples prepared starting from MCN are reported in Fig. 1(B). It is clear that the exfoliation did not destroy the tri-s-triazine structure of g-C_3N_4. All the reflections corresponding to (100), (101), (002), (300), and (004) crystal planes, in fact, are retained even after treatment at 540 °C.

According to the thermal analysis (Fig. S7) the maximum decomposition rate of the pristine MCN can be observed at approximately 750 °C, while the exfoliated sample MCN_540 began to decompose at lower temperature, as indicated by the DTG peak centred at 700 °C. The lower thermal stability of the exfoliated carbon nitride could be attributed to formation of ammonia from the large amount of amino-groups, which prevents oxidation of the material.

FTIR spectroscopy confirmed the structure of the prepared carbon nitride samples. All the major bands responsible for the bonds vibration of the g-C_3N_4 matrix, such as those attributable to heptazine ring (810 cm^{-1}) and to C—N—C and C—NH—C units (900–1800 cm^{-1}) remain almost unchanged for the as-prepared and exfoliated samples (Fig. S8).

The chemical state of the surface species of the exfoliated carbon nitride was investigated by XPS. All the major band positions for C, N, and O are virtually coincident with those reported for the thermally exfoliated carbon nitride [24,36], although it is useful, for the benefit of readers, to briefly highlight some important features which play a role in the present study. Deconvolution of the N 1s XPS peak obtained for the pristine MCN reveals contributions from three different nitrogen species (Fig. 3A).

The most intense peak centred at 398.4 eV is due to the C—N=C groups of the tri-s-triazine network, while the other bands at 400.0 eV and 401.1 eV can be assigned to N—$(C)_3$ groups and C—N—H linkages, respectively. The integrated intensity ratio of N—$(C)_3$ and C—N=C signals reflects the polymerization degree of the carbon nitride [38]. According to the deconvolution data (Table S1), the thermal exfoliation favours the increase of this ratio by completing the thermal polymerization process and eliminating uncondensed NH_2 species. All the deconvoluted XPS peaks show reasonable half-width at half-height (HWHM) values below 1 eV, however it can be noticed a significant peak broadening in the spectra of MCN_520 and MCN_540, probably resulting from the appearance of some additional contributions to the N 1s signal coming from the oxidized g-C_3N_4 fragments (Table S1).

The C 1s peak in all of the carbon nitride spectra is dominated by the contribution having a maximum at 288.0 eV, corresponding to the carbon of the N—C=N groups of tri-s-trizaine network (Fig. 3B). The second largest band observed at 284.8 eV can be attributed to the sp^2 bonded carbon of C—C bonds deriving from the adventitious hydrocarbon of the XPS instrument. The presence of C—N—H is witnessed by the small maximum at 286.1 eV. The peak near 289.7 eV in the spectrum of MCN can be attributed to C=O bonds of the carbonate species and it is due to the reaction of surface basic sites of the carbon nitride surface with atmospheric CO_2 (Fig. 3B). A HWHM value of this maximum is lower for MCN_450 sample and the signal completely disappears in the spectra of the samples treated at t ≥500 °C giving rise to a new contribution centred at 289.2 eV, which increases by increasing the g-C_3N_4 exfoliation temperature (Fig. 3B, Table S1). According to Li et al. [39], the latter maximum can be attributed to the oxidized carbon nitride surface, where sp^2-hybridized carbon is directly bonded to O atom. O 1s spectra support this hypothesis because the peak at 531.8 eV (C=O bonds) in the spectrum of pristine MCN is shifted to 532.5 eV (C—O) in that of MCN_540 (Fig. 3C).

The effect of the exfoliation on SSA was negligible for temperatures below 450 °C, in fact, only a twofold increase of this value was observed for MCN_450 with respect to g-C_3N_4, whilst the corresponding value ranged from 154 to 169 m^2g^{-1} for the samples treated at t ≥500 °C. All of the adsorption isotherms correspond to IV-type with H3 hysteresis loop indicating the presence of large mesopores, as reported in Fig. S9.

TEM images showing the typical morphology of the bulk and thermally exfoliated carbon nitride are reported in Fig. 4. The pres-

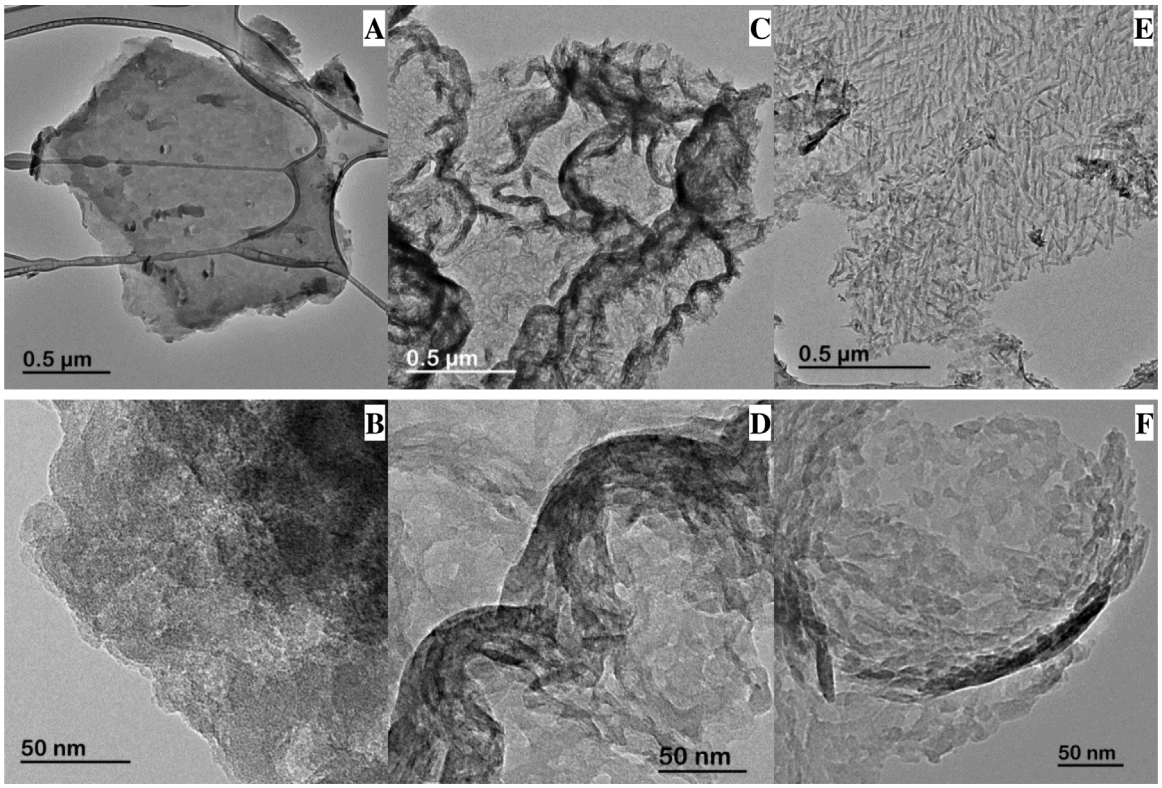

Fig. 4. TEM images of some selected samples: MCN (A) and (B), MCN_520 (C) and (D) and MCN_540 (E) and (F).

ence of large sheet-like particles of g-C_3N_4 showing no porosity is a feature of the material synthesized by thermal condensation of melamine (Fig. 4(A) and (B)). The thermal treatment under oxidant atmosphere results in disaggregation of the carbon nitride particles, which is probably due to the thickening and separation of layers caused by increasing treatment temperature (Fig. 4(C) to (F)).

Relatively large voids found between the particles are likely responsible for the appearance of a hysteresis loop in the N_2 adsorption-desorption isotherms (Fig. S9).

A significant blue shift of the absorption edge was observed for the thermally treated samples (Fig. S10), in good agreement with data previously reported for the exfoliated carbon nitride [36]. The band-gap energy increased from 2.73 eV for the as-prepared g-C_3N_4 to 2.90 eV for the sample exfoliated at 540 °C (Table 1). This change in the electronic properties of the material could be explained by the quantum confinement effect, which occurs as the result of separation of carbon nitride layers [24].

3.2.2. *Photocatalytic oxidation of HMF by using the exfoliated g-C_3N_4*

The increase of the SSA of the exfoliated carbon nitride samples resulted in a more efficient light absorption compared to the pristine MCN, thus the optimal amount of the photocatalysts was determined to be 50 mg according to radiometry measurements. The improved textural properties of MCN_500, MCN_520 and MCN_540 were also responsible for somewhat higher HMF adsorption (about 3%).

The photocatalytic HMF partial oxidation by using the thermo-exfoliated samples is reported in Fig. 5.

The observation of Fig. 5(A) and (B) indicates that the degradation rate of HMF was always higher than the formation rate of FDC for all of the samples tested. This finding indicates that the degradation of HMF proceeded at least by two parallel reactions, one of which gave rise to formation of FDC. Due to the fact that only FDC and small amounts of FFA (deriving from the further oxidation of FCD) were found as the products, it is likely that a parallel reaction gave rise to the complete mineralization of HMF by the formation of adsorbed open-chain aliphatic compounds. However, this work was not aimed to fully characterize the intermediates, most of which were present only as traces in the bulk of solution.

The HMF conversion rate grew with the increase of the thermal treatment temperature and SSA values, therefore it is not surprising that the slight enhancement of the SSA observed for MCN_450 with respect to the pristine MCN sample ($14\,m^2\,g^{-1}$ versus $7\,m^2\,g^{-1}$) did not improve the photocatalytic efficiency of carbon nitride (Fig. 5(A)). The drastic increase of the HMF conversion observed in the presence of the samples thermally treated at $t \geq 500$ °C, which reached the highest value of 69% in the presence of MCN_540 sample, along with the increase of the initial reaction rate by 2.5 times compared to that of the MCN sample (Table 1), could be related to the enhanced SSA of the thermally treated photocatalysts. However, the high reactivity of the exfoliated g-C_3N_4 cannot be explained only by taking into account its textural properties, because no direct correlation between these two parameters was found (see the sharp increase of the initial reaction rate observed in the presence of the sample with the higher SSA, Figs. S11A and B).

The XPS study indicates that the treatment under oxidative conditions modifies the functionality of the carbon nitride surface. The increased polymerization degree, the removal of NH_2 uncondensed basic sites playing the role of the CO_2 adsorption centres and the formation of C—O bonds on the g-C_3N_4 surface, probably account for a more efficient charge separation and interaction with a polar substrate. Moreover, the exfoliation led to band-gap broadening of g-C_3N_4, implying the increase of the conduction band potential and possibly the formation of reactive species *via* the reductive pathway [40]. Thus, this property could influence the oxidation rate and the selectivity of HMF conversion (Fig. S11C and D).

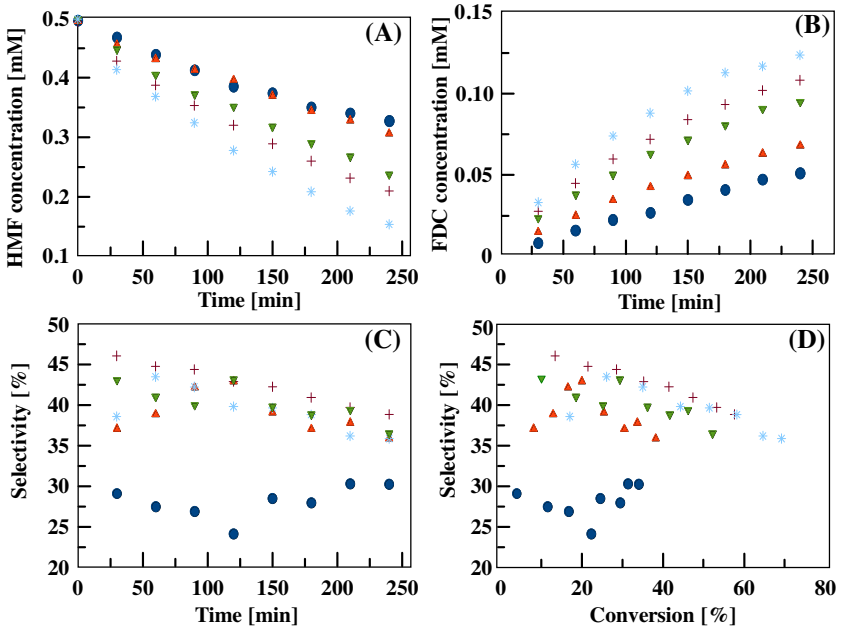

Fig. 5. HMF degradation (A); formation of FDC (B) and selectivity to FDC versus irradiation time (C) or selectivity to FDC versus HMF conversion (D) in the presence of the non exfoliated MCN (●), MCN_450 (▲), MCN_500 (▼), MCN_520 (+) and MCN_540 (✳).

The evolution of FDC gradually slowed down with time, due to the continuously decreasing concentration of HMF in the reaction medium, but the degradation of the substrate still prevailed over the FDC decomposition (Fig. 5(B)).

A satisfactory selectivity near 30% was found also in the presence of the pristine MCN (Fig. 5(C) and (D)) and it was noticeably higher than that reported for the TiO_2-assisted HMF photooxidation [16]. The thermal treatment of g-C_3N_4 at 450 °C did not significantly affect the activity of the photocatalyst, but the selectivity to FDC formation improved. XPS results indicate only the presence of small changes, possibly due to the elimination of the carbonate species adsorbed on the g-C_3N_4 basic sites. Such moieties interfere with the charge separation process, increasing the contribution of the reactive species which unselectively can decompose HMF. The selectivity to FDC formation reached its highest values (ca. 45%) for MCN_520 and MCN_540 samples and it was virtually identical after the same extent of conversion of HMF (Fig. 5(D)). Moreover, it decreased by increasing the conversion, because the product was subjected to further oxidative attacks, which gave rise to its decomposition, but it did not go down below 35% even after 69% of HMF conversion (Fig. 5(D)). High selectivity values observed for the exfoliated carbon nitride samples were also confirmed by GC–MS data (Fig. S12A and B).

FFA formed continuously during the photooxidation of HMF in the presence of MCN and the exfoliated carbon nitride samples (Fig. S13A). Similarly to the case of bulk g-C_3N_4 materials, the extent of FFA virtually depended only on that of FDC derived from HMF oxidation, regardless of the type of the catalyst used (Fig. S13 B).

In addition to the photolysis, the photocatalytic degradation of FDC could also take place, although the latter reaction was not significant. The inability of carbon nitride to produce $OH^\bullet$ radicals by direct interaction of electron-holes with water, did not favour the degradation of FDC, making HMF partial oxidation the prevailing process. Indeed, only about 35% of FDC decomposed after 4 h, conversely 69% of HMF was converted in the same time in the presence of MCN_540 (See Fig. S14).

The application of a set of scavengers helped to evaluate the contribution of different reaction pathways to the HMF decomposition and selectivity to FDC, as reported in Fig. 6 and in Fig. S15.

According to many reports [41,42], *tert*-butyl alcohol is an efficient $OH^\bullet$ scavenger. Its addition to the reaction mixture resulted in a minor change of HMF conversion rate while the selectivity remained unchanged. Therefore, one can suppose that the presence of hydroxyl radicals was not determinant for the HMF partial oxidation. When the reaction was carried out in anhydrous aprotic organic solvents, higher values of selectivity were usually achieved [31–33]. Under such conditions, the oxidation could proceed only *via* the direct interaction of the substrate and/or its intermediates with the photoproduced pairs on the photocatalyst surface or with $O_2^{\bullet-}$ radicals. The photooxidation of HMF in acetone resulted in much lower conversion rate, but it gave higher selectivity, which was due to the absence of unselective $OH^\bullet$ radicals and H_2O_2 (Fig. 6). Whether the substrate is decomposed *via* the direct electron-hole interaction was tested by the addition of sodium formate as a hole scavenger, which gave rise to a decrease of the HMF conversion to a significant extent, but also slightly enhanced the selectivity to FDC formation. Spasiano et al. [43] reported that the addition of cupric ions during the partial photooxidation of benzyl alcohol in water and TiO_2 under anaerobic conditions can promote the selectivity towards benzaldehyde formation. In that way it was established that the dominant process responsible for the selectivity of benzyl alcohol involves the formation of e^-- h^+ pairs. A similar experiment in the presence of carbon nitride resulted in a complete inhibition of the reaction. Cupric ions, indeed, can efficiently scavenge electrons, but the potential of the holes is unsuitable to oxidize HMF selectively. The application of *p*-benzoquinone as $O_2^{\bullet-}$ radical scavenger indicated that superoxide radicals were mainly responsible for the partial oxidation of HMF to FDC. Benzoquinone effectively consumed $O_2^{\bullet-}$ radicals hindering their interaction with HMF and yielding almost no selectivity to FDC formation.

Unexpectedly, the reaction did not completely stop under anaerobic conditions (N_2), although no electron scavengers were present (see Figs. 6 and S15). Almost 20% of HMF decomposed after 4 h of irradiation, and no significant selectivity to FDC was observed. The absence of any selectivity is in accordance with the absence of $O_2^{\bullet-}$ radicals, while the observed decomposition of the substrate could be explained by considering that terminal functional groups

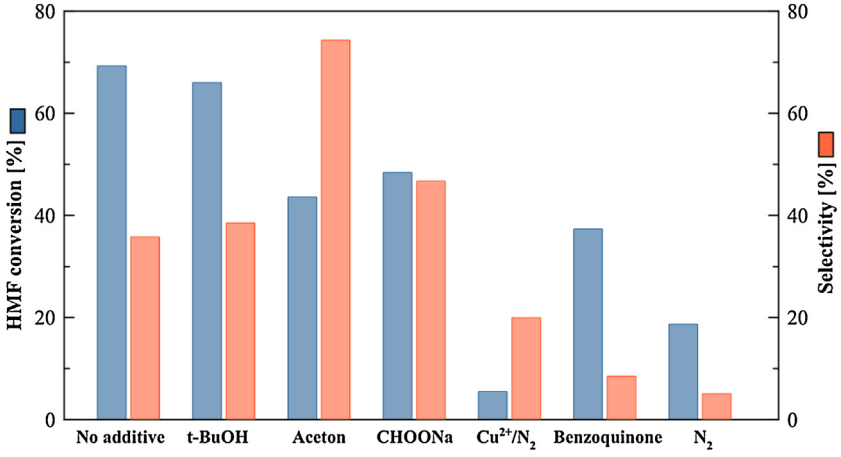

Fig. 6. Effect of scavengers (of charges and/or radicals) or of the solvent (acetone instead of water) on the HMF conversion and the corresponding selectivity to FDC after 240 min of irradiation in the presence of MCN_540.

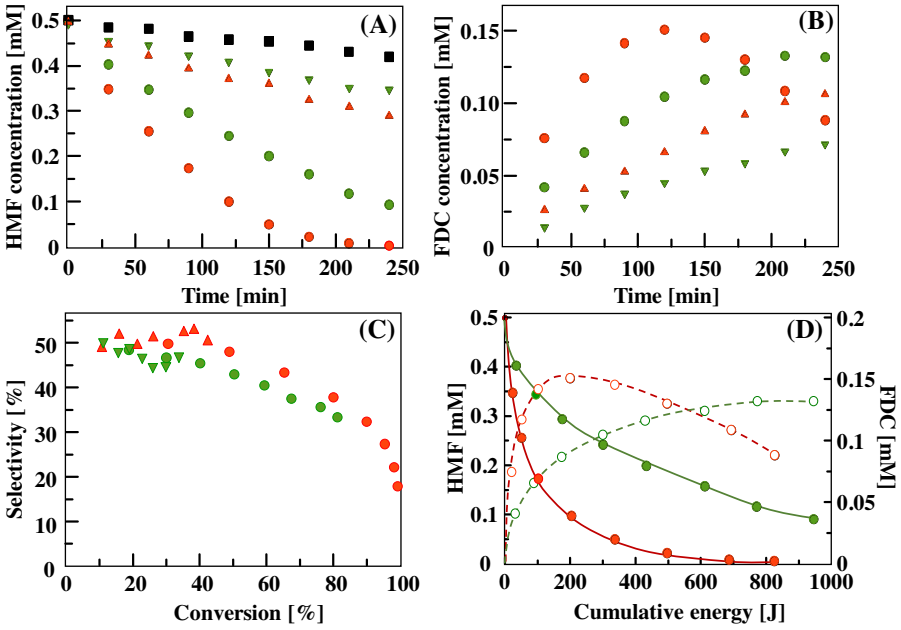

Fig. 7. HMF degradation (A); FDC formation versus irradiation time (B); selectivity of the reaction to FDC versus HMF conversion (C) and evaluation of HMF and FDC concentrations as a function of the cumulative energy entering the reactor for a reaction carried out under natural solar light irradiation (D). Symbols refer to a homogeneous photolysis experiment (■) or to runs carried out in the presence of MCN_520 or MCN_540 samples with (▼), (▲) and without (●), (●) a 1 M $NaNO_2$ filter. Empty symbols represent the FDC concentration during the solar experiment.

and/or adsorbed surface species on the photocatalyst could induce some extent of electron-hole separation.

Therefore, we confirm that, as in the case of photooxidation of aromatic alcohols in organic media [31], superoxide radicals formed *via* the reduction of molecular oxygen by the photogenerated electrons are the reactive species mainly responsible for the HMF partial oxidation to FDC in water. Zhang et al. reported the major role played by $O_2^{\bullet-}$ in the partial oxidation of aromatic alcohols to aldehydes with a selectivity higher than 96% by using Bi_2WO_6 as the photocatalyst in aqueous phase [44]. The higher selectivity values with respect to that obtained in this work could be attributed to the more stable benzene rings of the studied substrate molecules in Ref. [44], compared to the pentatomic furanic ring of HMF.

In order to test the stability of the catalyst some experiments were performed by reusing one of the best materials (MCN_520) in a series of four consecutive runs. The results reported in Fig. S16 indicate that the catalyst maintained ca. the same performance during all of the runs for both the conversion of HMF (57–58%) and the selectivity versus FDC formation (38–41%).

3.2.3. *Solar photo-oxidation of HMF by using exfoliated g-C_3N_4*

It is generally accepted that absorption of light by a photocatalyst extended as much as possible to the visible range can contribute to its better performance under a natural solar irradiation. However, many photocatalysts based on N-TiO_2 and g-C_3N_4 are able to utilize only a small portion of the visible irradiation, thus contributing slightly to the total photocatalytic activity of the material when sunlight is used. In this work, under solar irradiation the exfoliated carbon nitride samples showed a significantly higher activity than that observed using the UV-lamps of the laboratory set-up (see Figs. 5 (A) and 7 (A)). Notably, despite the band gap values of MCN_540 and MCN_520 were 2.90 and 2.79 eV, respectively, the latter was not more active even with the $NaNO_2$ filter cutting-off UV irradiation

(Fig. 7). The decreased activity of the carbon nitride at λ > 400 nm indicated, contrarily to what reported in some literature [34,45], that UV-light played a determinant role in the activation of the g-C_3N_4 at least under the experimental conditions used in this work (Fig. 7A and Table 1).

By observing the formation of FDC in the presence of MCN_540 photocatalyst (see Fig. 7(B)), it can be noticed that its concentration was maximum after about 2 h of irradiation and then it began to decline. This finding can be attributed to the decomposition of most of the HMF which was preferentially photooxidized by the carbon nitride.

The selectivity to FDC formation was somewhat higher under solar irradiation reaching about 50% after 40% conversion (Fig. 7(C)) by using MCN_520 and MCN_540, compared to experiments performed under UV-lamps irradiation. The use of a UV-filter did not significantly change the selectivity, although it reduced the HMF conversion and the photolysis of substrate and product. This finding indicates that the HMF partial oxidation by using carbon nitride occurred mainly under UV irradiation, and consequently the reaction data were plotted versus the cumulative energy entering the reactor between 315 and 400 nm. Fig. 7(D) reports the reactivity data in Fig. 7(A) and (B) for runs carried out in the presence of MCN_520 and MCN_540 samples versus the cumulative energy, E, entering the reactor [46]. The E value allows to compare photoreactivity results obtained under natural sunlight irradiation with different photocatalysts, and it was calculated by measuring the natural solar irradiance with a radiometer.

4. Conclusions

Graphitic carbon nitride demonstrated an outstanding selective photocatalytic performance in aqueous medium and in the absence of organic solvents. High selectivity of g-C_3N_4 in partial photooxidation of HMF to FDC was mainly due to its inability to generate unselective hydroxyl radicals, instead promoting the formation of highly efficient dehydrogenating $O_2^{\bullet-}$ species by reaction of electrons with atmospheric O_2. The main drawback of the carbon nitride, i.e its low specific surface area, was successfully overcome by implementing a facile thermal exfoliation procedure, which allowed not only to increase the reaction rate, but also to eliminate from the g-C_3N_4 surface uncondensed NH_2 sites, which were discovered to be detrimental for the partial photooxidation of HMF to FDC. The proposed material enabled to achieve 45% selectivity to FDC formation, which is higher than that (22%) reported by using TiO_2. The photocatalytic experiments under natural solar light irradiation showed that, despite the band gap energy of the carbon nitride allows utilization of a small portion of visible light, the UV fraction of the solar spectrum contributed to a greater extent to the excitation of the photocatalytic material. It was observed also that the exfoliated g-C_3N_4 showed even better activity and selectivity to FDC formation under real outdoor illumination, reaching 50% at 40% of HMF conversion in aqueous medium. The above results suggest that this material is a promising catalyst for application in the biomass-related compounds valorisation.

Acknowledgements

University of Oviedo gratefully acknowledges financial support from the MINECO (MAT2013-40950-R), FEDER-FICyT (GRUPIN14-060) and CTQ2014-52956-C3-1-R. IK thanks for the support the Ministry of Education and Science of the Russian Federation (grant No 16.2674.2014/K).

Appendix A. Supplementary data

Supplementary data associated with this article can be found, in the online version, at http://dx.doi.org/10.1016/j.apcatb.2016.11.049.

References

[1] D. Murzin, O. Simakova (Eds.), Biomass Sugars for Non-Fuel Applications, 1st ed., RSC, Cambridge, 2016.
[2] A.S. Amarasekara, D. Green, L.D. Williams, Renewable resources based polymers: synthesis and characterization of 2,5-diformylfuran-urea resin, Eur. Polym. J. 45 (2009) 595–598.
[3] Z. Hui, A. Gandini, Polymeric schiff bases bearing furan moieties, Eur. Polym. J. 28 (1992) 1461–1469.
[4] Y. Kanetaka, S. Yamazaki, K. Kimura, Preparation of poly(ether ketone)s derived from 2,5-furandicarboxylic acid by polymerization in ionic liquid, Macromolecules 49 (2016) 1252–1258.
[5] T.S.A. Heugebaert, C.V. Stevens, C.O. Kappe, Singlet-oxygen oxidation of 5-hydroxymethylfurfural in continuous flow, ChemSusChem 8 (2015) 1648–1651.
[6] B. Liu, Y. Ren, Z. Zhang, Aerobic oxidation of 5-hydroxymethylfurfural into 2,5-furandicarboxylic acid in water under mild conditions, Green Chem. 17 (2015) 1610–1617.
[7] L. Ozcan, P. Yalcin, O. Alagoz, S. Yurdakal, Selective photoelectrocatalytic oxidation of 5-(hydroxymethyl)-2-furaldehyde in water by using Pt loaded nanotube structure of TiO_2 on Ti photoanodes, Catal. Today 281 (2017) 205–213.
[8] J. Ma, Z. Du, J. Xu, Q. Chu, Y. Pang, Efficient aerobic oxidation of 5-hydroxymethylfurfural to 2,5-diformylfuran, and synthesis of a fluorescent material, ChemSusChem 4 (2011) 51–54.
[9] C. Carlini, P. Patrono, A.M.R. Galletti, G. Sbrana, V. Zima, Selective oxidation of 5-hydroxymethyl-2-furaldehyde to furan-2,5-dicarboxaldehyde by catalytic systems based on vanadyl phosphate, Appl. Catal. A 289 (2005) 197–204.
[10] V. Augugliaro, M. Bellardita, V. Loddo, G. Palmisano, L. Palmisano, S. Yurdakal, Overview on oxidation mechanisms of organic compounds by TiO_2 in heterogeneous photocatalysis, J. Photochem. Photobiol. C 13 (2012) 224–245.
[11] G. Palmisano, E. García-López, G. Marcí, V. Loddo, S. Yurdakal, V. Augugliaro, L. Palmisano, Advances in selective conversions by heterogeneous photocatalysis, Chem. Commun. 46 (2010) 7074–7089.
[12] X. Lang, X. Chen, J. Zhao, Heterogeneous visible light photocatalysis for selective organic transformations, J. Chem. Soc. Rev. 43 (2014) 473.
[13] J.C. Colmenares, W. Ouyang, M. Ojeda, E. Kuna, O. Chernyayeva, D. Lisovytskiy, S. De, R. Luque, A.M. Balu, Mild ultrasound-assisted synthesis of TiO_2 supported on magnetic nanocomposites for selective photo-oxidation of benzyl alcohol, Appl. Catal. B 183 (2016) 107–112.
[14] I. Tamiolakis, I.N. Lykakis, G.S. Armatas, Mesoporous CdS-sensitized TiO_2 nanoparticle assemblies with enhanced photocatalytic properties: selective aerobic oxidation of benzyl alcohols, Catal. Today 250 (2015) 180–186.
[15] C.J. Li, G.R. Xu, B. Zhang, J.R. Gong, High selectivity in visible-light-driven partial photocatalytic oxidation of benzyl alcohol into benzaldehyde over single-crystalline rutile TiO_2 nanorods, Appl. Catal. B 115–116 (2012) 201–208.
[16] S. Yurdakal, B.S. Tek, O. Alagoz, V. Augugliaro, V. Loddo, G. Palmisano, L. Palmisano, Photocatalytic selective oxidation of 5-(hydroxymethyl)-2-furaldehyde to 2,5-furandicarbaldehyde in water by using anatase, rutile, and brookite TiO_2 nanoparticles, ACS Sustain. Chem. Eng. 1 (2013) 456–461.
[17] S. Yin, J. Han, T. Zhou, R. Xu, Recent progress in g-C_3N_4 based low cost photocatalytic system: activity enhancement and emerging applications, Catal. Sci. Technol. 5 (2015) 5048–5061.
[18] Y.W. Zhang, J.H. Liu, G. Wu, W. Chen, Porous graphitic carbon nitride synthesized via direct polymerization of urea for efficient sunlight-driven photocatalytic hydrogen production, Nanoscale 4 (2012) 5300–5303.
[19] K. Wang, Q. Li, B. Liu, B. Cheng, W. Ho, J. Yu, Sulfur-doped g-C_3N_4 with enhanced photocatalytic CO_2-reduction performance, Appl. Catal. B 176–177 (2015) 44–52.
[20] Y. Wang, Y. Di, M. Antonietti, H. Li, X. Chen, X. Wang, Excellent visible-light photocatalysis of fluorinated polymeric carbon nitride solids, Chem. Mater. 22 (2010) 5119–5121.
[21] Z. Yang, Y. Zhang, Z. Schnepp, Soft and hard templating of graphitic carbon nitride, J. Mater. Chem. A 3 (2015) 14081–14092.
[22] X. Dong, F. Cheng, Recent development in exfoliated two-dimensional g-C_3N_4 nanosheets for photocatalytic application, J. Mater. Chem. A 3 (2015) 23642–23652.
[23] J. Xu, L. Zhang, R. Shi, Y. Zhu, Chemical exfoliation of graphitic carbon nitride for efficient heterogeneous photocatalysis, J. Mater. Chem. A 1 (2013) 14766–14772.
[24] P. Niu, L. Zhang, G. Liu, H.M. Cheng, Graphene-Like carbon nitride nanosheets for improved photocatalytic activities, Adv. Funct. Mater. 22 (2012) 4763–4770.
[25] X. Wang, S. Blechert, M. Antonietti, Polymeric graphitic carbon nitride for heterogeneous photocatalysis, ACS Catal. 2 (2012) 1596–1606.

[26] F. Su, S.C. Mathew, L. Mohlmann, M. Antonietti, X. Wang, S. Blechert, Aerobic oxidative coupling of amines by carbon nitride photocatalysis with visible light, Angew. Chem. 50 (2011) 657–660.
[27] X. Chen, J. Zhang, X. Fu, M. Antonietti, X. Wang, Fe-g-C_3N_4-Catalyzed oxidation of benzene to phenol using hydrogen peroxide and visible light, J. Am. Chem. Soc. 131 (2009) 11658–11659.
[28] Z. Ding, X. Chen, M. Antonietti, X. Wang, Synthesis of transition metal-modified carbon nitride polymers for selective hydrocarbon oxidation, ChemSusChem 4 (2011) 274–281.
[29] X.H. Li, X. Wang, M. Antonietti, Solvent-free and metal-free oxidation of toluene using O_2 and g-C_3N_4 with nanopores: nanostructure boosts the catalytic selectivity, ACS Catal. 2 (2012) 2082–2086.
[30] X.H. Li, J.S. Chen, X. Wang, J. Sun, M. Antonietti, Metal-free activation of dioxygen by graphene/g-C3N4 nanocomposites: functional dyads for selective oxidation of saturated hydrocarbons, J. Am. Chem. Soc. 133 (2011) 8074–8077.
[31] F. Su, S.C. Mathew, G. Lipner, X. Fu, M. Antonietti, S. Blechert, X. Wang, Mpg-C_3N_4-Catalyzed selective oxidation of alcohols using O_2 and visible light, J. Am. Chem. Soc. 132 (2010) 16299–16301.
[32] S. Verma, R.B.N. Baig, M.N. Nadagouda, R.S. Varma, Selective oxidation of alcohols using photoactive VO@g-C_3N_4, ACS Sustain. Chem. Eng. 4 (2016) 1094–1098.
[33] J. Xu, L. Luo, G. Xiao, Z. Zhang, H. Lin, X. Wang, J. Long, $C_3N_3S_3$ Polymer/graphene hybrids as metal-free catalysts for selective photocatalytic oxidation of benzylic alcohols under visible light, ACS Catal. 4 (2014) 3302–3306.
[34] J. Xu, L. Luo, G. Xiao, Z. Zhang, H. Lin, X. Wang, J. Long, Layered $C_3N_3S_3$ polymer/graphene hybrids as metal-free catalysts for selective photocatalytic oxidation of benzylic alcohols under visible light, ACS Catal. 4 (2014) 3302–3306.
[35] B. Long, Z. Ding, X. Wang, Carbon nitride for the selective oxidation of aromatic alcohols in water under visible light, ChemSusChem 6 (2013) 2074–2078.
[36] F. Dong, Y. Li, Z. Wang, W.K. Ho, Enhanced visible light photocatalytic activity and oxidation ability of porous graphene-like g-C_3N_4 nanosheets via thermal exfoliation, Appl. Surf. Sci. 358 (2015) 393–404.
[37] F. Fina, S.K. Callear, G.M. Carins, J.T.S. Irvine, Structural investigation of graphitic carbon nitride via XRD and neutron diffraction, Chem. Mater. 27 (2015) 2612–2618.
[38] S. Gu, J. Xie, C.M. Li, Hierarchically porous graphitic carbon nitride: large-scale facile synthesis and its application toward photocatalytic dye degradation, RSC Adv. 4 (2014) 59436–59439.
[39] J. Li, B. Shen, Z. Hong, B. Lin, B. Gao, Y. Chen, A facile approach to synthesize novel oxygen-doped g-C3N4 with superior visible-light photoreactivity, Chem. Commun. 48 (2012) 12017–12019.
[40] H. Zhang, L.H. Guo, L. Zhao, B. Wan, Y. Yang, Switching oxygen reduction pathway by exfoliating graphitic carbon nitride for enhanced photocatalytic phenol degradation, J. Phys. Chem. Lett. 6 (2015) 958–963.
[41] T. Xu, P.V. Kamat, K.E. O'shea, Mechanistic evaluation of arsenite oxidation in TiO_2 assisted photocatalysis, J. Phys. Chem. A. 109 (2005) 9070–9075.
[42] M.B. Gilliard, C.A. Martín, A.E. Cassano, M.E. Lovato, Reaction kinetic model for 2,4-dichlorophenoxyacetic acid decomposition in aqueous media including direct photolysis, direct ozonation, ultraviolet C and pH enhancement, Ind. Eng. Chem. Res. 52 (2013) 14034–14048.
[43] D. Spasiano, L.P.P. Rodriquez, J.C. Olleros, S. Malato, R. Marotta, R. Andreozzi, TiO_2/Cu(II) photocatalytic production of benzaldehyde from benzyl alcohol in solar pilot plant reactor, Appl. Catal. B: Environ. 136–137 (2013) 56–63.
[44] Y. Zhang, Y.J. Xu, Bi_2WO_6: A highly chemoselective visible light photocatalyst toward aerobic oxidation of benzylic alcohols in water, RSC Adv. 4 (2014) 2904–2910.
[45] G. Mamba, A.K. Mishra, Graphitic carbon nitride (g-C3N4) nanocomposites: a new and exciting generation of visible light driven photocatalysts for environmental pollution remediation, Appl. Catal. B: Environ. 198 (2016) 347–377.
[46] V. Augugliaro, E. García-López, V. Loddo, S. Malato-Rodriguez, I. Maldonado, G. Marcì, R. Molinari, L. Palmisano, Degradation of lyncomycin in aqueous medium: coupling of slar photocatalysis and membrane separation, Sol. Energy 79 (2005) 402–408.